Implementation of the Methodology of Coupled Modelling of Aerodynamics and Strength to Determine the Onset Speed of the Bending-Torsional Flutter of the Wing Console

Anastasia Rymanova[1,*], *Evgenia* Guseva[1], and *Vitaly* Gunchin[1]

[1]Moscow Aviation Institute (National Research University), Moscow, Russia

Abstract. Time-domain motion simulations using the averaged Navier-Stokes Euler and Reynolds equations were performed for an AGARD 445.6 wing in transonic flow. These simulations were compared with experimental results as well as with the solution in the frequency domain using a method based on the fast Fourier transform. The model matches in frequencies and shapes with experiment.

1 Introduction

Flutter is a phenomenon of dynamic aeroelasticity caused by the interaction of inertial, elastic and aerodynamic forces. The oscillation mode of the structure determines the possibility of a flutter and depends on many parameters, including the flight speed. In this paper, using numerical modelling methods, the interaction of several simultaneously resonating oscillation modes at different velocity pressures and Mach numbers is considered on the example of the classical experiment Agard 445.6.

2 Computational Dynamics Modelling

In the experiment [1], a wing console model was used with an elongation λ = 1.6525, a narrowing = 0.6576 and a sweep along the quarter chord $X_{1/4}$=45º. The profile used is NACA 65A004. The model is made of laminated red wood. To reduce stiffness, holes were drilled in the model along the normal to the plane of the chord. The holes obtained as a result of drilling were filled with foam to preserve the theoretical contour. The model was loaded with the help of an incoming air flow. During the experiment, the Reynolds number varied from Re = 0.5 million to Re = 6.7 million. The wing console was fixed to the wall of the wind tunnel without imitation of the fuselage in such a way that the root part of the console was immersed in the boundary layer, in order to minimize the effect of the joint of the model with the wall on the results of the experiment [2]. The model was equipped with strain gauges mounted externally at the root of the wing console and oriented in such a way

* Corresponding author: RymanovaAN@mai.ru

as to distinguish the bending and torsion of the wing. The strain gauge signals were recorded on a multichannel oscilloscope and displayed on a cathode ray oscilloscope to help determine the flutter onset. The displacements of the wing console were additionally analysed using video recordings with a frequency of 128 frames per second.

To construct a finite element model, the original geometric characteristics were preserved, and the equality of stiffness values was ensured by the reduced properties of the material [3] To simulate the constraints, an encastre was used on the side of the wing root chord [4]. The model consists of two finite element grids: a structural-power mesh, necessary for the perception of external loads [5], and an aerodynamic mesh, necessary for obtaining external aerodynamic loads and transferring them to a structural-power mesh [6]. The aerodynamic mesh used first-order quadrangular elements with an average face size of 2.5 mm. The structural and power mesh used hexagonal elements of the first order with an average face size of 5 mm.

At the initial stage, the validation of the finite element model of the wing console was carried out through modal analysis. The calculation methodology implemented in the CAE program is based on the following relation [7]:

$$\frac{\partial q_i^2}{\partial t_i^2} + \omega_0^2 q_i = 0 \tag{1}$$

where q_i – displacement components,

ω_0^2 – natural frequency.

As can be seen from the above relation, the modal analysis does not take into account the parameters of the external influence. There is also some overestimation of the values of natural frequencies caused by the fact that when constructing a finite element model, all the restrictions of displacement are considered ideal, which does not fully correspond to the conditions for fixing the physical model. The values of the natural frequencies of the wing console oscillations obtained using the finite element model exceed the values of the natural frequencies obtained experimentally by no more than 5%. The calculation results and the error are presented in Table 1.

Table 1. Comparison of natural frequencies obtained experimentally and using FEM

Mode number	Oscillation frequency (experiment), Hz	Natural frequency (modal analysis), Hz	Error, %
1	9.60	9.61	0.13
2	38.17	39.69	3.80
3	48.35	48.44	0.20
4	91.54	95.82	4.45
5	118.11	119.47	1.14

Next, a CFD calculation was carried out. The determination of the pressure values on the surface of the model is carried out by numerical simulation [8]. The calculations were performed by the computational gas dynamics method – the solution of the Reynolds-averaged Navier-Stokes equations [9,10,11]:

$$\begin{cases} \dfrac{\partial \rho}{\partial t} + \dfrac{\partial u_i}{\partial x_i} = 0 \\ \dfrac{\partial \rho u_i}{\partial t} + \dfrac{\partial \rho u_j u_i}{\partial x_j} = -\dfrac{\partial p}{\partial x_i} + \dfrac{\partial}{\partial x_i}\left(2\mu \mathrm{S}_{ij} - \rho u_i u_j\right) + p f_i \\ \dfrac{\partial}{\partial t}\left[\rho\left(\mathrm{e} + \dfrac{1}{2}u_i u_j\right)\right] + \dfrac{\partial}{\partial x_j}\left[\rho u_j\left(\mathrm{h} + \dfrac{1}{2}u_i u_j\right)\right] = \dfrac{\partial}{\partial x_j}\left[u_j\left(2\mu \mathrm{S}_{ij} - \rho u_i u_j\right)\right] - \dfrac{\partial q_j}{\partial x_j} \end{cases} \quad (2)$$

where $u_{i,j}$ $\boldsymbol{u_{i,j}}$ – velocity components,

ρ – density,

μ – viscosity,

f_i – a force per unit of volume such as gravitational force,

e – is specific internal energy,

h – enthalpy,

q_j – heat flux vector.

Based on the initial geometric characteristics of the experimental setup, a CAD model is constructed, shown in Figure 1.

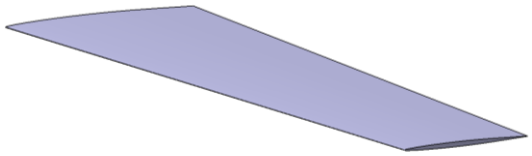

Fig. 1. CAD model of the experimental model.

The calculated area is a hemisphere. Sym (the plane of symmetry of the hemisphere) and Freestream (the outer boundaries of the computational domain) are used as boundary conditions. The surface of the experimental setup is a Wall boundary condition (a wall without slippage). The external boundaries of the computational domain, the boundaries of the computational domain at the surface of the model and the resolution of the wall area are shown in Figures 2, 3.

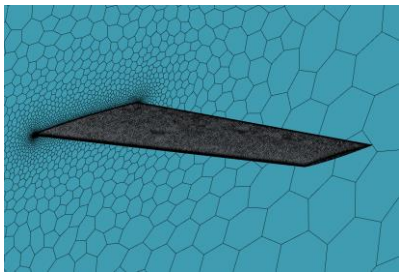

Fig. 2. Boundaries of the computational domain (model surface).

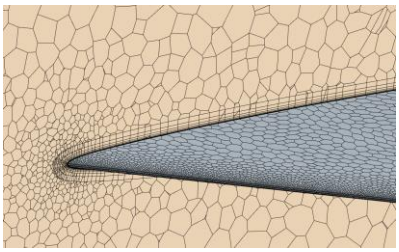

Fig. 3. Resolution of the wall area (prismatic layers).

The experimental model does not have drainage holes and pressure sensors, so the measurement of the aerodynamic forces acting on the model is also not provided. Thus, it is not possible to validate the CFD solver for this experiment. Figure 4 shows the nature of the distribution of the pressure coefficient over the surface, obtained by numerical simulation (M = 1.141, angle of attack = 0º), in comparison with the results of the authors [12,13,14].

Visualization of the pressure distribution over the surface of the model is shown in Figure 5.

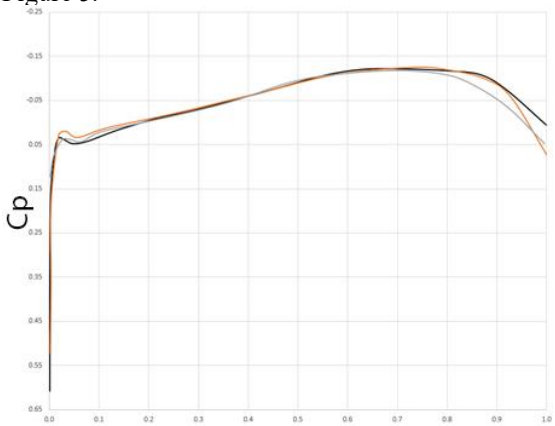

Fig. 4. Distribution of the pressure coefficient in the 26% span section.

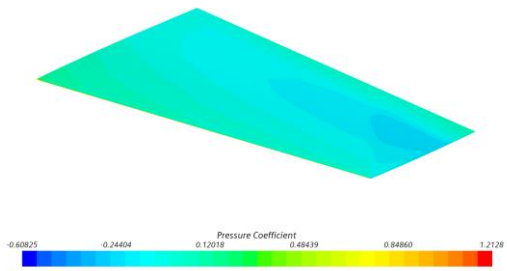

Fig. 5. Distribution of the pressure coefficient over the surface.

Next, the loads from the CFD solver are transferred to the finite element model and an implicit dynamic analysis is started. The equation for this case is given below [7]:

$$\frac{\partial q_i^2}{\partial t^2} + 2\beta \frac{\partial q_i}{\partial t} + \omega_0^2 q_i = 0 \tag{3}$$

where β – viscous damping.

In contrast to the equation used in the modal analysis, the above ratio takes into account the parameters of the external influence in the form of damping [15]. The calculation duration is 0.75 s. The time integrator parameter alpha = 0. At the beginning of the step, the wing is twisted by a moment of 10000 N, acting relative to the normal to the plane of the end rib. The increment value is fixed and is 0.005 s. The load and boundary conditions applied to the model are shown in Figure 6.

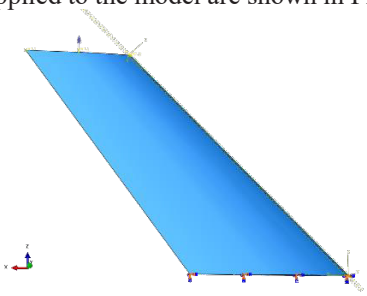

Fig. 6. Load and boundary conditions in implicit dynamic analysis**.**

3 Flutter analysis

Figures 7-10 below show the dependences of sensor displacements on time at different Mach numbers. Further, to calculate the frequencies of wing oscillation during flight, calculations were carried out in the frequency domain. As a result of the work, peak frequency values were allocated for each of the 4 Mach numbers.

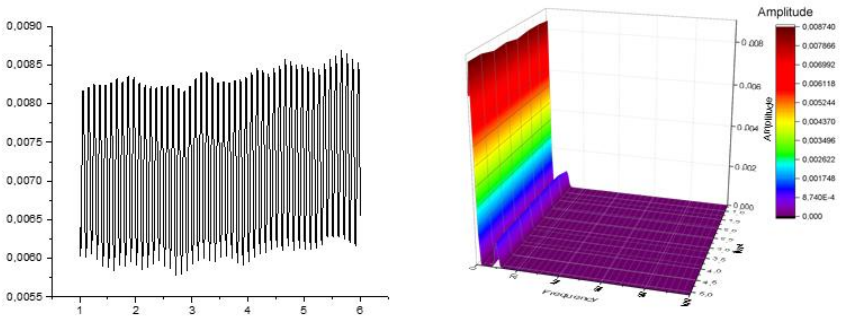

Fig. 7. The dependence of sensor 1 movement on time and the results of the short-term Fourier transforms at M=0.3.

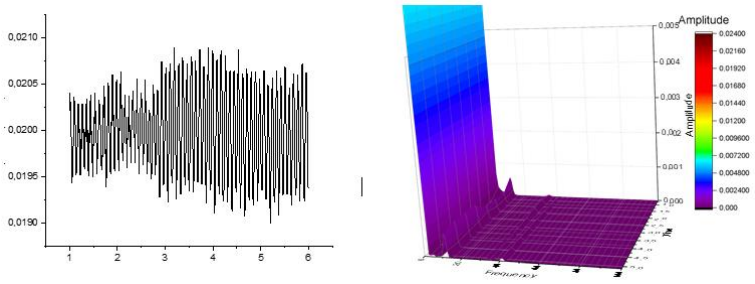

Fig. 8. The dependence of sensor 1 movement on time and the results of the short-term Fourier transforms at M=0.5.

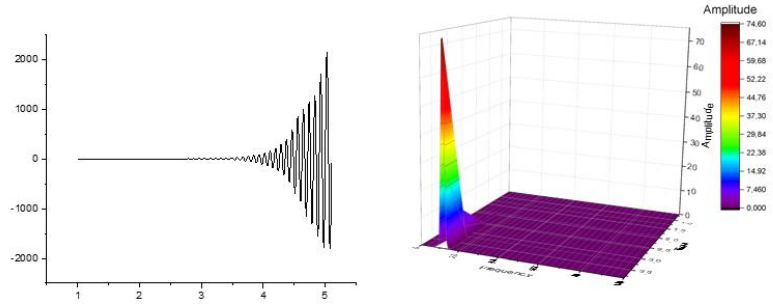

Fig. 9. The dependence of sensor 1 movement on time and the results of the short-term Fourier transforms at M= 0.7.

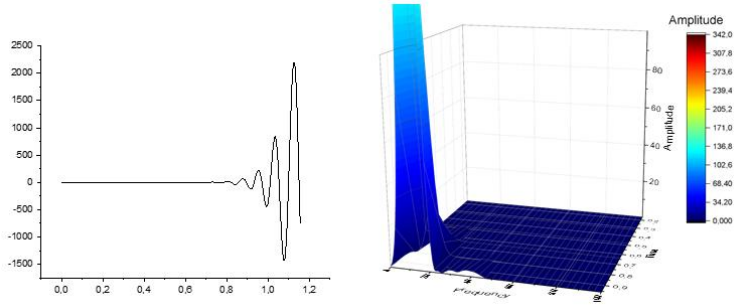

Fig. 10. The dependence of sensor 1 movement on time and the results of the short-term Fourier transforms at M=1.1.

4 Conclusion

As you can see, with an increase in the Mach number, several frequencies begin to affect the nature of the movement due to the interaction of several oscillation modes. The flutter goes from bending to bending-torsional.

Based on the results of the fast Fourier transform, it can be traced that the value of the main peak frequency increases with the growth of the Mach number.

As a result of the work, it can be concluded that with an increase in the Mach number, the number and values of frequencies that determine the oscillation mode of the console

increases, which leads to a change in the shape of the flutter. It also follows from the calculations that the oscillation frequencies in the Mach number range from 0.03 to 1.1 may differ from the natural frequencies by up to 4 Hz.

References

1. Yates Jr, E. C., (1987) 'Agard standard aeroelastic configurations for dynamic response. candidate configuration i.-wing 445.6'.
2. Yerokhin, A., Deniskin, Y. Airfoil smoothing using unconditional optimization. AS (2023). https://doi.org/10.1007/s42401-023-00232-7.
3. Strizhius, V.E., Turbin, N.V. Fatigue strength estimates for composite wing panels of prospective supersonic transport aircraft. AS (2023). https://doi.org/10.1007/s42401-023-00210-z.
4. Yurkovich, R., "Status of unsteady aerodynamic prediction for flutter of high-performance aircraft", Journal of Aircraft, Vol. 40, No. 5, 2003, pp. 832-842.
5. McCain, W. E., "Measured and calculated airloads on a transport wing model", Journal of Aircraft, Vol. 22, No. 4, 1985, pp. 336-342
6. Zenkevich O. (1975) Finite element method in technology. – M: Mir.
7. Fershing G. (1984) Aeroelasticity Basics. – M.: Mechanical engineering.
8. Gordnier, R.E. and Melville, R.B., "Transonic flutter simulations using an implicit aeroelastic solver", Journal of Aircraft, Vol. 37, No. 5, 2000, pp. 872-879.
9. Silva. P.A.S., Morais, M.V.G. Fluid Structure Interaction on AGARD 445.6 wing at Mach 0.9 Proceedings of the XXXVII Iberian Latin-American Congress on Computational Methods in Engineering Suzana Moreira Avila (Editor), ABMEC, Braslia, DF, Brazil, November 6-9, 2016
10. Guo Tongqing. A CFD/CSD model for aeroelastic calculations of large-scale wind turbines. Science China Technological Sciences, January 2012, 56(1).
11. Lee-Rausch, E. M. & Batina, J. T., 1993. 'Calculation of agard wing 445.6 flutter using navier-stokes aerodynamics', AIAA paper pp. 3476,9–11.
12. M. Ozcatalbas, B. Acar and S. Uslu, Investigation of Aeroelastic Stability on AGARD 445.6 Wing at Transonic Regime. 2018 9th International Conference on Mechanical and Aerospace Engineering (ICMAE), Budapest, Hungary, 2018, pp. 565-569, doi: 10.1109/ICMAE.2018.8467693.
13. Yates, E. C., "AGARD standard aeroelastic configurations for dynamic response I-wing 445.6", AGARD Report 765, North Atlantic Treaty Organization, Group for Aerospace Research and Development, 1988.
14. Badcock, K. J., Woodgate, M. A. and Richards, B. E., "Direct aeroelastic bifurcation analysis of a symmetric wing based on the Euler equations", Technical Report 0315, Department of Aerospace Engineering, University of Glasgow, 2003.
15. Kamakoti, R., Shyy, W., 2004. 'Fluid–structure interaction for aeroelastic applications', Progress in Aerospace Sciences pp. 40,8,535–558.